Physica C 202 (1992) 51–60
North-Holland

PHYSICA C

Local structure of $Y_{1-x}Ca_xSr_2Cu_2GaO_7$ superconductors

J.P. Zhang [a,b], D.A. Groenke [a,c], H. Zhang [a,b], D.I. DeLoach [c], B. Dabrowski [a,d,e], K.R. Poeppelmeier [a,c], V.P. Dravid [a,b] and L.D. Marks [a,b]

[a] *The Science and Technology Center for Superconductivity, Northwestern University, Evanston, IL 60208, USA*
[b] *Department of Materials Science and Engineering, Northwestern University, Evanston, IL 60208, USA*
[c] *Department of Chemistry, Northwestern Universtity, Evanston, IL 60208, USA*
[d] *Materials Science Division, Argonne National Laboratory, Argonne, IL 60439, USA*
[e] *Northern Illinois University, DeKalb, IL, 60115, USA*

Received 20 July 1992

The variation in the average and local structure of the superconductor family $Y_{1-x}Ca_xSr_2Cu_2GaO_7$ as calcium is substituted for yttrium ($x=0.20$, 0.35, and 0.40) is presented and discussed. Electron microscopy and X-ray diffraction were the primary techniques employed. The local structure found by the use of electron microscopy and X-ray diffraction agrees with that previously derived from single crystal X-ray and neutron diffraction. The gallate can be confused with the three layer perovskite structure of YBCO ($YBa_2Cu_3O_7$) because of the similarity of $[011]_{Ga} \approx [100]_{YBCO}$ and $[010]_{Ga} \approx [110]_{YBCO}$ zones. However, the composition of all crystals examined were homogeneous on a 10–100 nm scale. It was also found that the twin structure varied as a function of the calcium content.

1. Introduction

There has been extensive research into compounds with copper–oxygen layers since the discovery of high-temperature superconductivity in the La–Ba–Cu–O system by Bednorz and Müller [1]. Many high-temperature superconductors have been discovered and they include compounds in the Y–Ba–Cu–O [2,3], Bi–Ca–Sr–Cu–O [4,5], Tl–Ba–Ca–Cu–O [6,7] and Pb–Sr–Ln–Cu–O [8] systems (Ln=La...Lu, Y). The common features of these superconducting compounds are copper–oxygen planes and a spacer layer between the planes that contains elements which are capable of variable valence. The copper–oxygen planes are important because they are considered the key to high-temperature superconductivity, but with the variable valence spacers charge transfer between the planes is possible. Recently a layered cuprate with a fixed oxidation state spacer was synthesized, $LnSr_2Cu_2GaO_7$ (Ln=La...Yb, Y); this compound contains copper–oxygen planes separated by gallium–oxide tetrahedra. Superconductivity is induced by p-doping and annealing in high-pressure oxygen atmosphere, i.e. $Y_{1-x}Ca_xSr_2Cu_2GaO_7$ [9].

The chemical and structural differences between the superconducting and nonsuperconducting states in $Y_{1-x}Ca_xSr_2Cu_2GaO_7$ are difficult to detect. So far most structural investigations have been X-ray and neutron diffraction, which are statistical averages of structural features that are relatively insensitive to low levels of impurities (<5%). Any impurities (<5%) will be more apparent when samples are examined using electron microscopy. By using microscopic techniques. a better understanding of the local structure of the compound and the structural changes caused by the high-pressure oxygen annealing can be obtained. We focus upon the average structure of these gallium-containing superconductors and demonstrate that the X-ray and neutron diffraction data is correct both in terms of the local structure and chemistry. In a later [10] paper we will discuss some rather unusual line defects that were also observed in the material and that may be important to the superconducting properties.

2. Experimental methods

Polycrystalline samples of $Y_{1-x}Ca_xSr_2Cu_2GaO_7$ and $YSr_{2-x}Ca_xCu_2GaO_7$ (x=0.00, 0.05, 0.10, 0.15, 0.20, 0.25, 0.30, 0.35 and 0.40) were synthesized from stoichiometric amounts of (Aldrich) Y_2O_3 (99.99%), $CaCO_3$ (99.995%), $SrCO_3$ (99.995%) CuO (99.99%) and Ga_2O_3 (99.99%). The samples were heated in air at 950°C for 3 weeks and were ground frequently. These samples were removed from the oven directly and quenched at room temperature. A portion of these samples was annealed under high-pressure oxygen and cooled at 2°C/min. The conditions for the annealing are as follows: for $Y_{0.80}Ca_{0.20}Sr_2Cu_2GaO_7$ the temperature was 910°C and the pressure was 200 bar, for $Y_{0.65}Ca_{0.35}Sr_2Cu_2GaO_7$ and $Y_{0.60}Ca_{0.40}Sr_2Cu_2GaO_7$ the conditions were 970° C and 500 bar.

X-ray powder diffraction measurements were obtained by the use of a Rigaku diffractometer equipped with Cu Kα radiation and a nickel filter. The data sets were collected by using a step width of 2θ=0.02° with a 10 s collection time and were suitable for Rietveld refinement. An internal standard of silicon (Aldrich, 99.9999%) was added for calibration purposes. The data sets were used to determine lattice constants by the use of Rietveld refinement.

For the electron microscopy we have primarily used powder samples that were dry crushed and dispersed onto holey carbon films. We have also checked the data with ion-beam thinned pressed and sintered pellets. A variety of microscopes and techniques were used in this study. Electron diffraction patterns as a function of angle (equivalent to single crystal X-ray patterns) were obtained using a Hitachi H700 operated at 200 kV. High resolution electron microscopy was performed using a Hitachi H9000 operated at 300 kV, with image simulations on Apollo workstations using the standard multislice approach. Careful chemical analysis and convergent beam electron diffraction was performed using a Hitachi HF 2000 operated at 200 kV.

3. Results

3.1. X-ray lattice parameters

A Rietveld refinement [11] of the powder X-ray diffraction data of $Y_{1-x}Ca_xSr_2Cu_2GaO_7$ and $YSr_{2-x}Ca_2Cu_2GaO_7$ was performed to determine the lattice parameters. The starting structural model for the powder X-ray refinement was based on the results of the neutron diffraction data of $HoSr_2Cu_2GaO_7$, which has been previously reported [6]. The structure of the compounds is shown in fig. 1. Lattice constants versus doping level are shown in figs. 2–4.

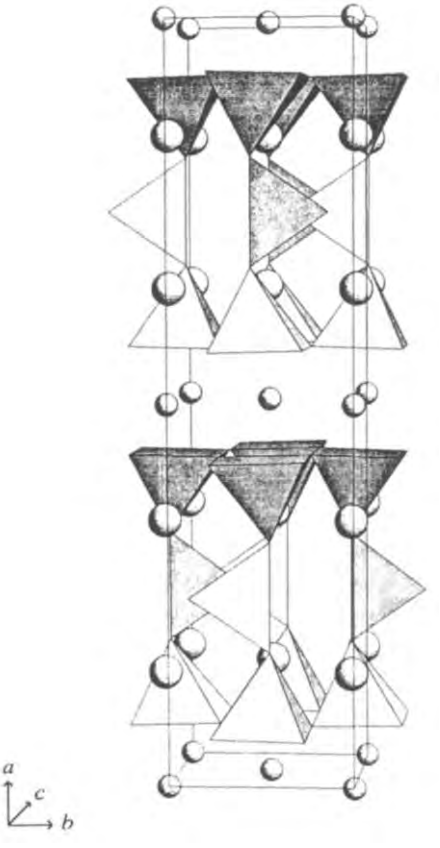

Fig. 1. Basic structure of the superconductor $Y_{1-x}Ca_xSr_2Cu_2GaO_7$. The small spheres represent yttrium and calcium, large spheres are strontium atoms, the square pyramids are CuO_5, and the tetrahedron are GaO_4.

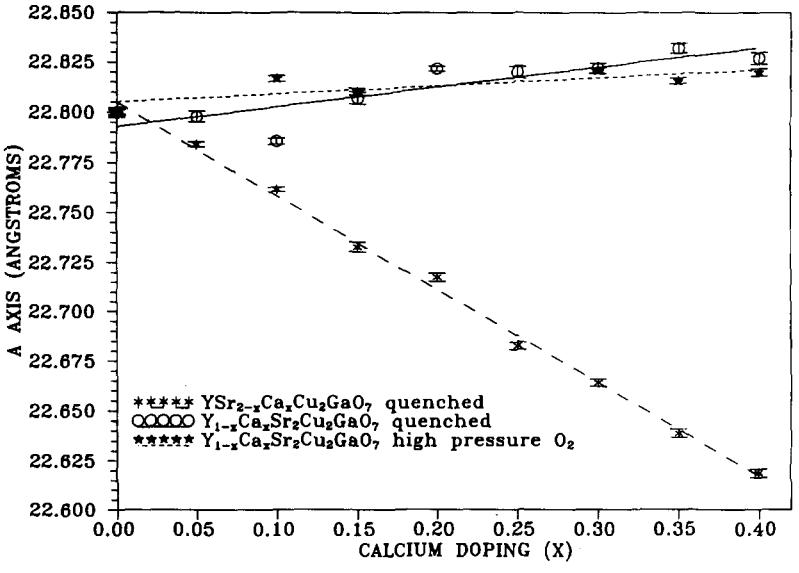

Fig. 2. Variations in *a*-axis for quenched $Y_{1-x}Ca_xSr_2Cu_2GaO_7$, quenched $YSr_{2-x}Ca_xCu_2GaO_7$ and high-pressure oxygen annealed (300 bar, 930°C) $Y_{1-x}Ca_xSr_2Cu_2GaO_7$.

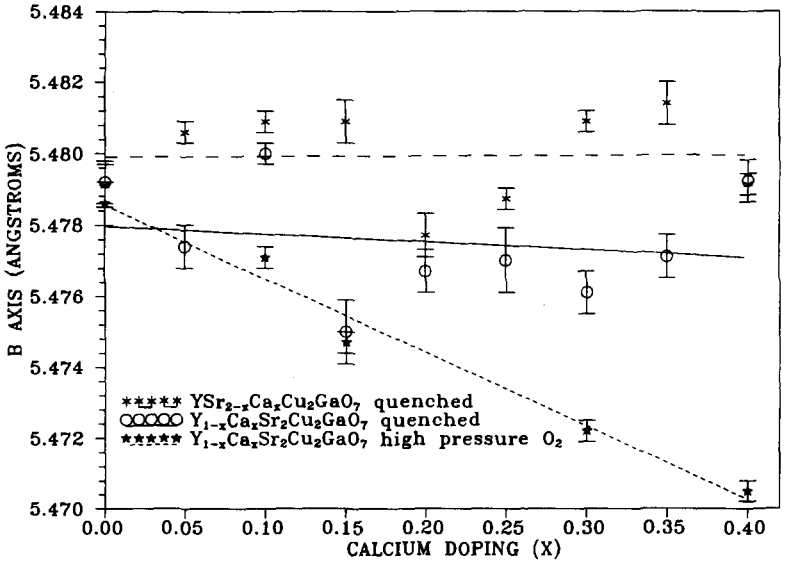

Fig. 3. Variations in *b*-axis for quenched $Y_{1-x}Ca_xSr_2Cu_2GaO_7$, quenched $YSr_{2-x}Ca_xCu_2GaO_7$, and high-pressure oxygen annealed (300 bar, 930°C) $Y_{1-x}Ca_xSr_2Cu_2GaO_7$.

3.2. Superconductivity

Superconductivity was detected in high-pressure annealed samples of $Y_{1-x}Ca_xSr_2Cu_2GaO_7$ ($x \geq 0.15$), by resistivity and susceptibility measurements that have been reported elsewhere [9,12]. In this work, the superconductors with $x=0.20$, 0.35 and 0.40 were selected for a microstructure study. The onset tem-

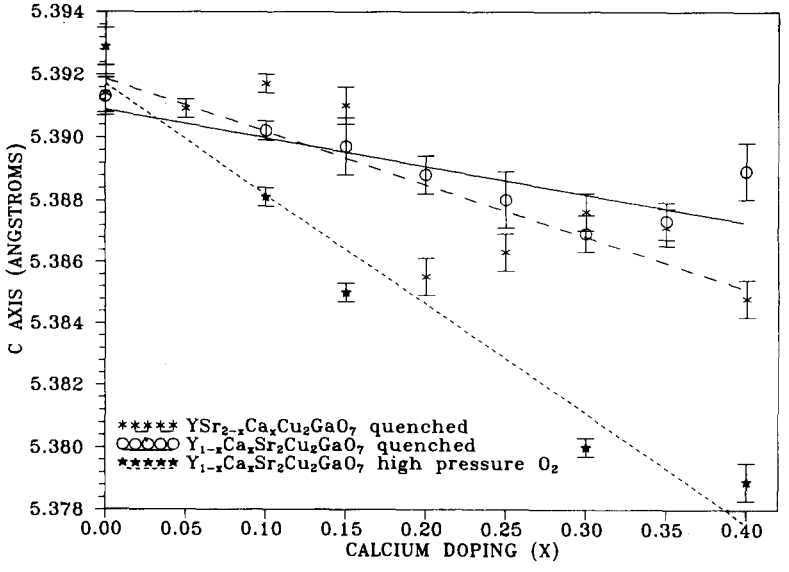

Fig. 4. Variations in *c*-axis for quenched $Y_{1-x}Ca_xSr_2Cu_2GaO_7$, quenched $YSr_{2-x}Ca_xCu_2GaO_7$, and high-pressure oxygen annealed (300 bar, 930°C) $Y_{1-x}Ca_xSr_2Cu_2GaO_7$.

perature for superconductivity, and the shielding fraction at 5 K are as follows: 26 K and 0.01%, 40 K and 18%, and 44 K and 15%, respectively. The difference in magnetic susceptibility between quenched and high-pressure oxygen annealed samples of $Y_{0.65}Ca_{0.35}Sr_2Cu_2GaO_7$ is shown in fig. 5.

3.3. Chemical composition

X-ray microchemical analyses show that the cation concentrations in each material are essentially spatially homogeneous on a 10–100 nm scale for all the compositions. Figure 6 shows a representative

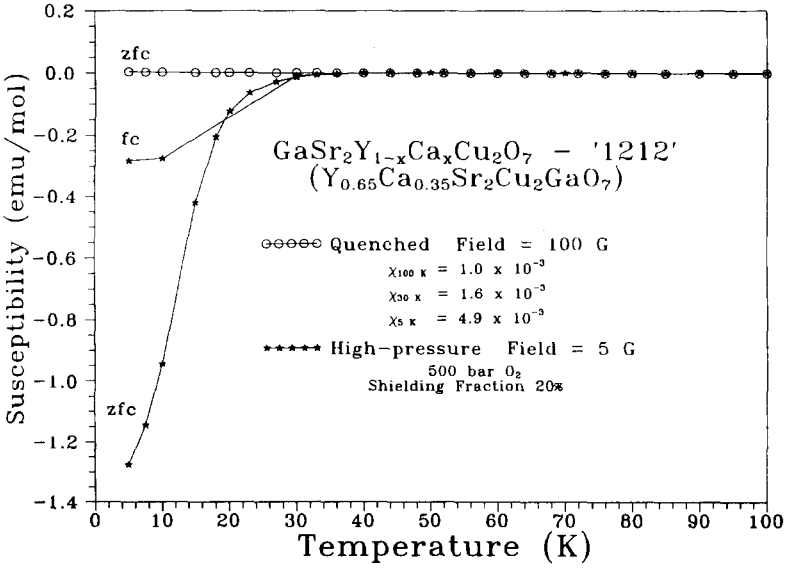

Fig. 5. Magnetic susceptibility of $Y_{0.65}Ca_{0.35}Sr_2Cu_2GaO_7$ quenched and high-pressure oxygen annealed.

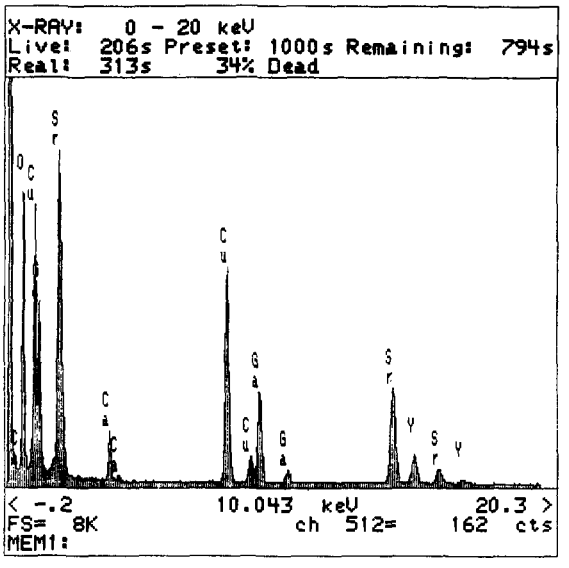

Fig. 6. EDX spectrum of the superconductor.

spectrum, which depicts the various elements in the appropriate proportions. X-ray diffraction showed the presence of impurity phases for $x \geq 0.30$ in $Y_{1-x}Ca_xSr_2Cu_2GaO_7$. Before high-pressure annealing the impurity was a mixture of $SrCuO_2$ (10%) and $Sr_{14-x}Ca_xCu_{24}O_{41}$ (7%). After the annealing there was only $Sr_{14-x}Ca_xCu_{24}O_{41}$ present, and the intensity of the major peak (located at 31.0° 2θ) is approximately six percent of the major peak for $Y_{1-x}Ca_xSr_2Cu_2GaO_7$.

3.4. Electron diffraction data

Diffraction patterns from all zones show the systematic absence $h+k+l=2n+1$. Examples from the four basic zones [100], [010], [001] and [011] are shown in fig. 7. In addition, the reflections $h=2n+1$ are forbidden in the [010] zone. These indicate the existence of an a-glide, so that the space group is either Ima2 (No. 46) or Imam (No. 74). To discriminate between these two, convergent beam electron diffraction patterns along the [100] zone were obtained as shown in fig. 8. The pattern indicates a diffraction group of m (one mirror plane only), so the point group of the crystal is mm2 (C_{2v}), and the space group Ima2.

One important point, which we will return to as well when we discuss the high resolution images, is that some of the zones are very similar to those for the $Yba_2Cu_3O_{7-\delta}$ [13] structure (YBCO). In particular, $[011] \approx [100]_{YBCO}$; $[010] \approx [110]_{YBCO}$. Figure 9 shows diffraction patterns along [021] obtained by tilting crystals either from the [011] zone by 18.3 degrees or from the [010] zone by 26.2 degrees. Along the [021] zone, the YBCO structure is not the same, and of seven crystals for which either the confused [011] or [010] zone diffraction patterns were obtained and also the unconfused [021] zone, none correlated to the YBCO structure. Of a total of 50 different grains where diffraction patterns (or with high-resolution images) were obtained, none corresponds to YBCO. We can rule out such an impurity for the source of the superconductivity.

For the [100] pattern in fig. 7(a) and the [021] zone in fig. 9, there are streaks along the b^*-axis [14]. This will be discussed in a subsequent paper [14].

3.5. High-resolution imaging

High resolution images taken along the [100], [010], [001] and [011] zones are shown in fig. 10. In all cases the images are completely consistent with image simulations (inset) calculated using the X-ray structure. The [011] and [010] zone images, as mentioned above, can easily be confused with a YBCO-like structure. However, the [100] zone clearly shows the roughly 5.4 Å square cell that is at 45 degrees to the simple perovskite cell and $\sqrt{2}\ a_p$ larger. In addition, the [001] zone image clearly shows the presence of the gallium containing layers (marked by lines) with a glide of $\frac{1}{2}$ [100]; the formation of a hexagonal feature in the image from the SrO–GaO–SrO sandwich is significantly sensitive to the local atomic structure.

3.6. Twins

The compound is orthorhombic, so it is not surprising to find that within single grains there are twins, see fig. 11. The twin plane, for all compositions, was {011}, but there was a distinct difference in the a-axis orientation; in the $x=0.20$ sample, the a-axes were predominantly parallel whereas in the $x=0.40$ sample they were predominantly orthogonal. Compared with that observed in YBCO, the twin

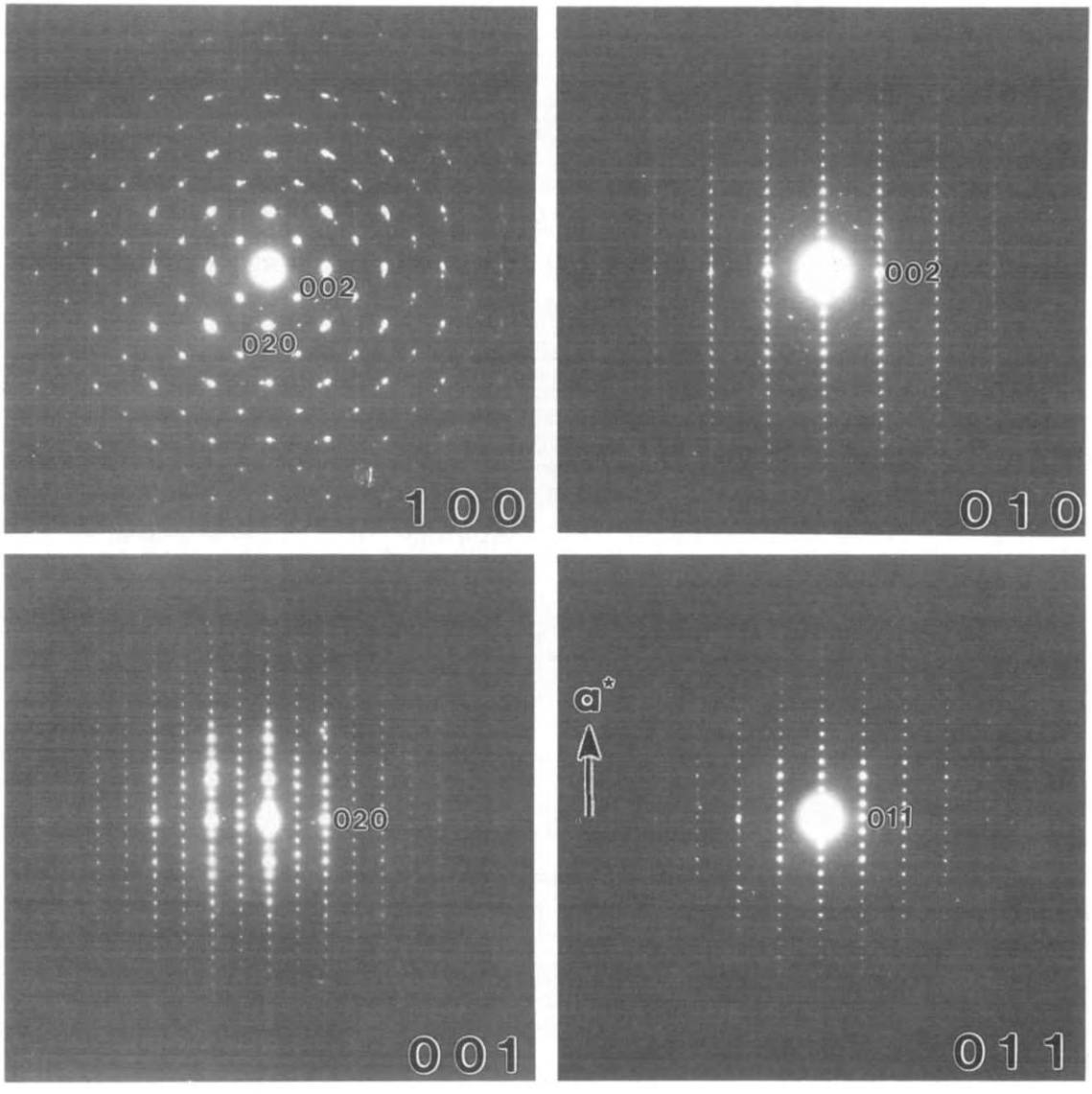

Fig. 7. Electron diffraction patterns along the [100], [010], [001] and [011] zones in (a) to (d), respectively, as discussed in the text.

plane in the parallel twin was rotated 45 degrees, whereas it remained the same in the orthogonal twin. It should be noted that based on group theory, the existence of twins within the grains implies a higher symmetry phase existing as the parent of the room-temperature orthorhombic phase, which will be discussed below.

4. Discussion

4.1. Structure–property relations

The two different calcium substitutions in $YSr_2Cu_2GaO_7$, aliovalent doping for the lanthanide atom ($Y_{1-x}Ca_xSr_2Cu_2GaO_7$) and the calcium–strontium solid solution ($YSr_{2-x}Ca_xCu_2GaO_7$), demonstrate the effects of the size of the A cations on lattice parameters in perovskite structures. The *a*-

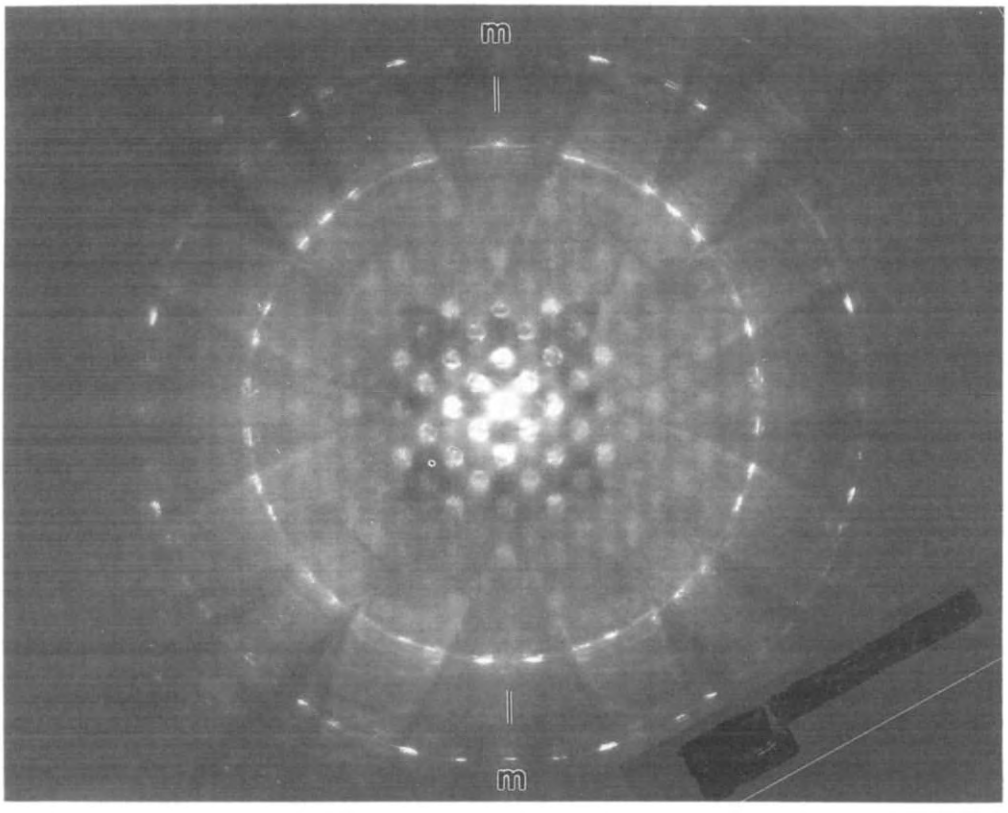

Fig. 8. Convergent beam electron diffraction pattern along [100].

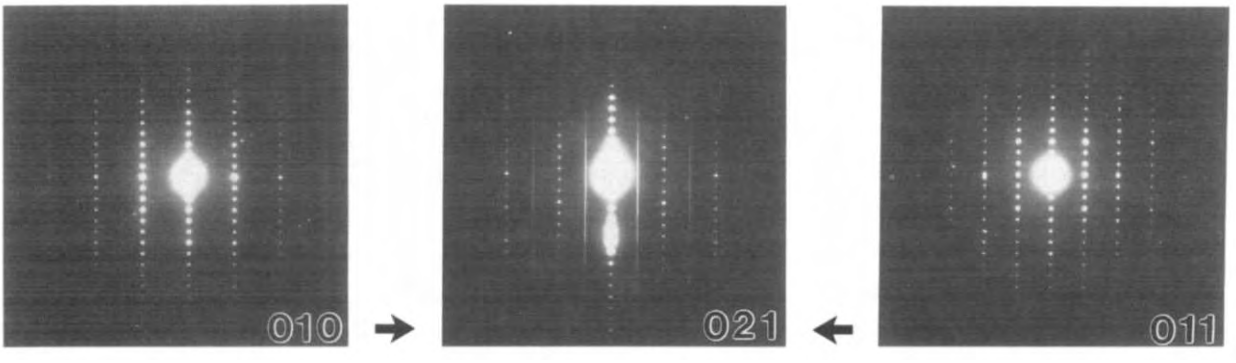

Fig. 9. Electron diffraction pattern along [021] obtained by tilting either 18.3° from [011] or 26.2° from [010].

axis shows the effect of the average size of the A cation in the lattice. when the yttrium (1.019 Å) [15] is replaced by calcium (1.12 Å) the average size of the A cations increases slightly, whereas the substitution of calcium for strontium (1.26 Å) decreases the average size. As shown in fig. 2, the *a*-axis decreases upon larger calcium substitution for strontium, whereas the *a*-axis increases slightly for the aliovalent doping for yttrium. Also the high pressure annealing does not affect the size of the *a*-axis in $Y_{1-x}Ca_xSr_2Cu_2GaO_7$.

The aliovalent doping was undertaken to oxidize

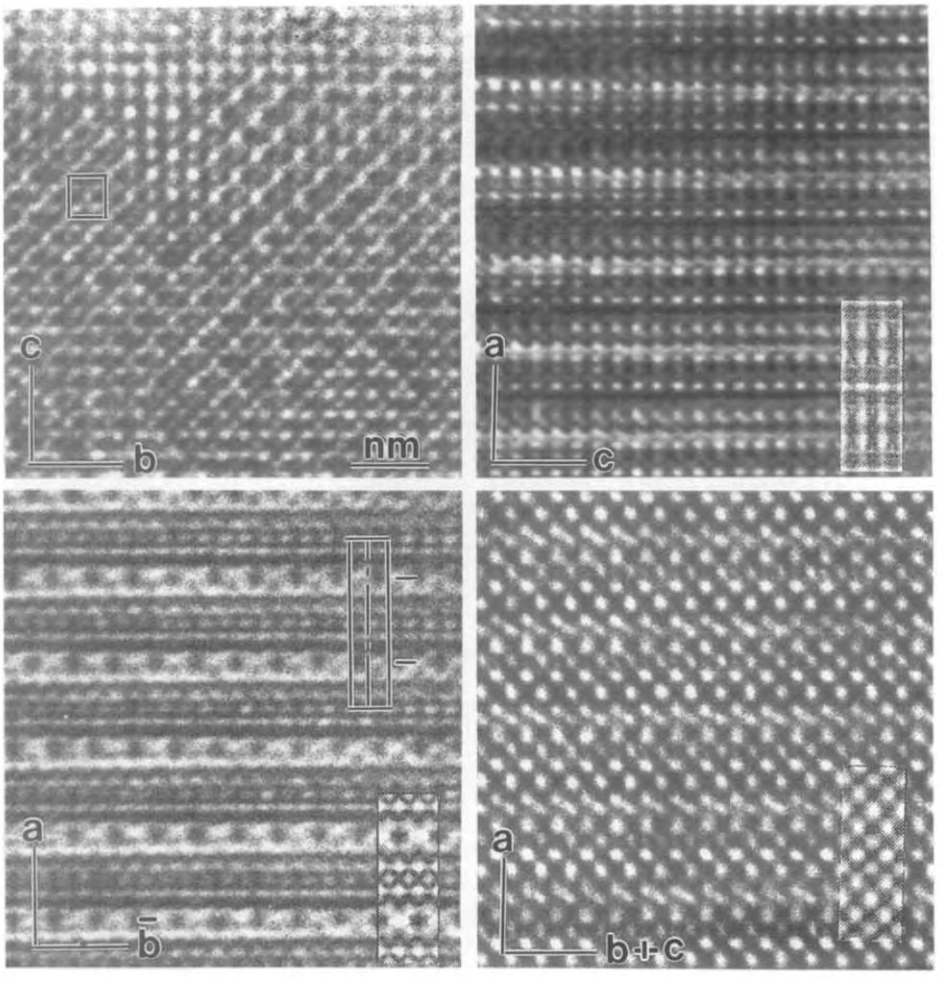

Fig. 10. High-resolution images along the [100], [010], [001] and [011] zones in (a) to (d) respectively, with the unit cell and the gallium planes marked as mentioned in the text and image simulations inset.

the compound into a superconductor. Providing there are no oxygen vacancies, oxidation should remove electrons from the antibonding $d_{x^2-y^2}$ orbitals and increase the overlap of the in-plane copper oxygen orbitals. As seen in figs. 3 and 4 the *b*- and *c*-axes, which contain the copper–oxygen planes, decrease after the high-pressure oxygen annealing, which is consistent with increased Cu $d_{x^2-y^2}$/O 2p overlap. The quenched samples do not change, most likely from oxygen defects caused by the quenching.

4.2. Microstructure

Twins are the products of a reduction in symmetry during a displacive phase transformation. Usually the ordered structure with lower symmetry is derived from a disordered or less ordered one at higher temperature [16]. The twinned relationship can be expressed by the loss of operations in the group–subgroup decomposition of the two related structures, and it can also be identified experimentally [17]. In other words, the geometrically oriented twins imply a disorder–order phase transition when the crystal is cooled down to a lower temperature. Similar to Ni_3Nb [18] and $YBa_2Cu_3O_{7-\delta}$ [13,19], we expressed the process of symmetry reduction in a point group from a high-temperature cubic perovskite to the room temperature orthorhombic phase

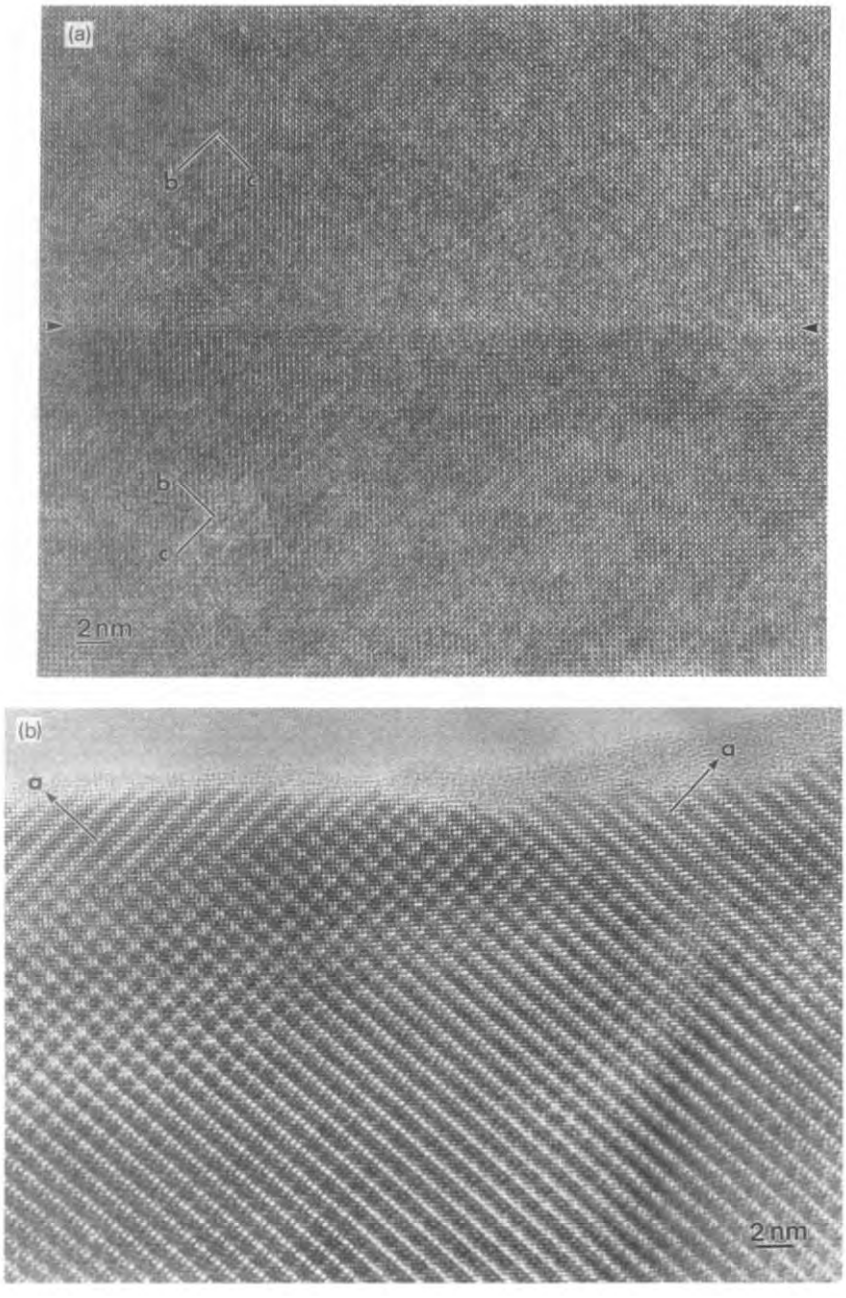

Fig. 11. High-resolution images of twins in (a) with the *a*-axis parallel and in (b) with the *a*-axis perpendicular.

in $Y_{1-x}Ca_xSr_2Cu_2GaO_7$ superconductors as

$$O_h\left(\frac{4}{m}\bar{3}\frac{2}{m}\right) \xrightarrow{C_3} D_{4h}\left(\frac{4}{m}\frac{2}{m}\frac{2}{m}\right) \xrightarrow{C_{4\to 2}} C_{2v}(mm2)\,,$$

where C_3 is the 3-fold rotation that is lost in the cubic to tetragonal transition, and $C_{4\to 2}$ is the reduction of the 4-fold rotation to 2-fold during the orthogonal deformation. In order to describe the

process clearly, a tetragonal D_{4h} structure is assumed as an "intermediate", but it does not necessarily exist. The loss of the operation C_3 implies the possible ordering of cations along all three [100] directions of the cubic perovskite , leading to the *a*-axis perpendicular domains of the orthorhombic structure. The $C_{4\to 2}$ operation implies the *a*-axis parallel domains along the ordering direction. Thus the observed domain structures imply a perovskite framework with randomly arranged cations at high temperature.

We have limited this paper to a description of the basic structure of this superconductor and the twin structures. All the data that we have shown here is based upon data from more than one crystal and is quite reproducible. Although there is no evidence of any YBCO-like material, particularly towards the high calcium content compositions there is a second impurity phase of Sr–Cu–O with variable calcium content in an composition similar to $Sr_{14-x}Ca_xCu_{24}O_{41}$ as studied by McCarron et al. [20]. There are also line defects whose density and local structure varied substantially with the stoichiometry, which wh will discuss in more detail elsewhere [7].

Acknowledgement

This work was supported by the NSF-DMR program through the Science and Technology Center for Superconductivity grant number NSF-DMR-8809854.

References

[1] J.G. Bednorz and K.A Müller, Z. Phys. B: Cond. Matt. 64 (1986) 189.
[2] M.K. Wu, J.R. Ashburn, C.J. Torng, P.H. Hor, R.L. Meng, L. Gao, Z. Huang, Y.Q. Wang and C.W. Chu, Phys. Rev. Lett. 58 (1987) 908.
[3] M.A. Beno, L. Soderholm, D.W. Capone, J.D. Jorgenson, I.K. Schuller, C.U. Segre, K. Zhang and J.D. Grace, Appl. Phys. Lett. 51 (1987) 57.
[4] C.W. Chu, J. Bechtold, L. Gao, P.H. Hor, Z.J. Huang, R.L. Meng, Y.Y. Sun, Y.Q. Wang and Y.Y. Xue, Phys. Rev. Lett. 60 (1988) 941.
[5] C. Greaves and T. Forgan, Nature (London) 332 (1988) 305.
[6] Z.Z. Sheng and AM. Hermann, Nature (London) 332 (1988) 138.
[7] M.A. Subramanian, J.B. Parise, J.C. Calabrese, C.C. Toradi, J. Gapalakrishnan and A.W. Sleight, J. Solid State Chem. 77 (1988) 192.
[8] R.J. Cava, B. Batlogg, J.J. Krajewski, L.W. Rupp, L.F. Schneemeyer, T. Siegrist, R.B. van Dover, P. Marsh, W.F. Peck, K. Gallagher, S.H. Glarum, J.H. Marshall, R.C. Farrow, J.V. Waszczak, R. Hull and P. Trevor, Nature (London) 336 (1988) 221.
[9] J.T. Vaughey, J.P. Theil, E.F. Hasty, D.A. Groenke, C.L. Stern, K.R. Poeppelmeier, B. Dabrowski, D.G. Hinks and A.W. Mitchell, Chem. Mater. 3 (1991) 935.
[10] J.P. Zhang et al., in preparation.
[11] D. Wiles, A. Sakthevel and R. Young, Rietveld Analysis Program-version DBWS-9006; School of Physics, Georgia Institute of Technology, Atlanta, GA, 1990.
[12] B. Dabrowski, P. Radaelli, D.G. Hinks, A.W. Mitchell, J.T. Vaughey, D.A. Groenke and K.R. Poeppelmeier, Physica C 193 (1992) 63.
[13] L.D. Marks, D.J. Li, H. Shibahara and J.P. Zhang, J. Electron Microsc. 8 (1988) 297.
[14] J.P. Zhang, H. Zhang, V.P. Dravid, L.D. Marks, D.A. Groenke, J.T. Vaughey, K.R. Poeppelmeier, B. Dabrowski, D.G. Hinks and A.W. Mitchell, to be presented at the 5APEM meeting, 2–5 August, Beijing, 1992.
[15] R.D. Shannon, Acta Crystallogr. A 32 (1976) 751.
[16] H. Wondraschek and W. Jeitchko, Acta Crystallogr. A 32 (1976) 664.
[17] G. van Tendeloo and S. Amelincks, Acta Crystallogr. A 30 (1974) 431.
[18] J.P. Zhang, H.Q. Ye, K.H. Kuo and S. Amelincks, Phys. Status Solidi A 93 (1986) 457.
[19] V.P. Dravid, C.E. Lyman and M.R. Notis, Appl. Phys. Lett. 52 (1988) 933.
[20] E.M. McCarron, III, M.A. Subramanian, J.C. Calabrese and R.L. Harlow, Mater. Res. Bull. 23 (1988) 1355.